The origin of the Younger Dryas cold period

Hans Renssen[1*], Aurélien Mairesse[2], Hugues Goosse[2], Pierre Mathiot[3], Oliver Heiri[4], Didier M. Roche[1,5], Kerim H. Nisancioglu[6], Paul J. Valdes[7]

1) Department of Earth Sciences, VU University Amsterdam, The Netherlands
2) Earth and Life Institute, Georges Lemaître Centre for Earth and Climate Research, Université catholique de Louvain, Louvain-la-Neuve, Belgium
3) British Antarctic Survey, Natural Environment Research Council, Cambridge, UK
4) Institute of Plant Sciences and Oeschger Centre for Climate Change Research, University of Bern, Bern, Switzerland
5) Laboratoire des Sciences du Climat et de l'Environnement, IPSL, Laboratoire CEA-INSU-UVSQ-CNRS, Gif-sur-Yvette, France
6) Bjerknes Centre for Climate Research and Department of Earth Sciences, University of Bergen, Norway
7) School of Geographical Sciences, University of Bristol, UK

*Corresponding author : h.renssen@vu.nl, phone +31 20 5987376, fax +31 20 5989941

The Younger Dryas (YD) is a prominent climate cooling phase that disrupted the overall warming trend in the North Atlantic region during the last deglaciation[1-6]. The YD provides unprecedented evidence for abrupt climate change[7-9], making it a crucial period for our understanding of the climate system sensitivity to perturbations. The classical explanation for this sudden cooling is a shut-down of the Atlantic Meridional Overturning Circulation (AMOC) due to meltwater discharges[10-13]. However, recently this classical mechanism has been challenged by alternative explanations, including strong negative radiative forcing[14] and a shift in the atmospheric circulation[15]. Here we evaluate these different forcings in coupled climate model experiments constrained by data assimilation and find that the YD climate signal as registered in proxy evidence is best explained by a combination of processes: weakened AMOC, moderate negative radiative forcing and altered atmospheric circulation. We conclude that an AMOC shut down or any of the other individual mechanisms does not provide a plausible explanation for the YD cold period. This indicates that the triggers for abrupt climate change are more complex than suggested so far. Studies on the climate system response to perturbations should account for this complexity.

Proxy data from the North Atlantic region indicate that the YD started 12.9 thousand years ago (ka) with a strong cooling that abruptly terminated the Allerød warm phase[3-4,16]. Summer temperatures in Europe dropped sharply by several degrees[4,16], during a time when the orbitally-induced summer insolation at 60°N was close to its 11 ka maximum (i.e. 47 Wm^{-2} above the modern level[17]). Concurrently, the North Atlantic Ocean also experienced a cooling of several degrees[4]. However, the YD cooling was not global, as the Southern Hemisphere extratropics were not cooler or even slightly warmer than during Allerød time[4,18]. Thus, a mechanism is required that explains all these specific features of the YD cold period.

The main hypothesis for the YD cause is a catastrophic drainage of Lake Agassiz, leading to freshwater-induced AMOC collapse and abrupt reduction of the associated northward heat transport[10]. Indeed, model simulations[19] suggest that this mechanism fits very well with several characteristics of the YD, including the abruptness of the YD start, and its specific spatial pattern with strongest cooling in the North Atlantic region and relatively warm conditions in Antarctica. However, reconstructions of the AMOC strength do not support a full collapse during YD time[20-21], thus questioning the validity of this hypothesis. In addition, several alternative mechanisms have been proposed for the trigger of the YD. A prominent, but highly debated, hypothesis suggests that the YD was triggered by an extraterrestrial impact[14], leading to enhanced atmospheric dust levels and reduced radiative forcing, possibly in combination with increased ice-sheet melt. Other suggestions include a large solar minimum[22] triggering strong cooling and a wind shift associated with changes in ice sheet configuration[15]. Hence, despite decades of intense research, the forcing mechanism of the YD is still debated.

In this study, we analyse different forcing mechanisms for the YD by combining climate model simulations with proxy-based reconstructions, mainly consisting of European July temperatures and annual sea surface temperatures (SSTs) in the North Atlantic Ocean (see Methods and Supplementary Information). These proxy-based reconstructions indicate that European summers were on average 1.7°C cooler than in the preceding Allerød period at 13ka (Fig. 1, Extended Data Fig. 1), with the strongest reduction (up to 4.0°C) in NW Europe, diminishing towards the southeast (0.5°C cooling). The annual SST reconstructions suggest that the North Atlantic was on average 2.4°C cooler at mid latitudes (Fig. 1, Extended Data Fig.1), while further north the cooling was even stronger (-5°C).

To analyze the possible mechanism for the YD, we performed a set of experiments in which a 13 ka Allerød reference state was perturbed (Table 1). This reference state was obtained by running the model with persistent appropriate 13 ka background forcings, consisting of orbital parameters, ice sheets, land-sea distribution, and atmospheric trace gas levels. To represent the background melting of the Laurentide and Scandinavian Ice Sheets, we also applied freshwater fluxes of 0.05 Sv (1 Sv equals $1x10^6$ m^3s^{-1}) in both the NW Atlantic and the Norwegian Sea during 500 yrs (see Supplementary Information). This freshwater forcing resulted in local shut-down of Labrador Sea deep convection in agreement with palaeoceanographic evidence[23] and reduced AMOC strength (from 24 to 16 Sv, Extended Data Fig. 4). All these forcings were maintained in our perturbation experiments.

We constrained part of the simulations by applying a data-assimilation (DA) method (particle filter, see Supplementary Information), enabling us to find the estimate of both the system state and the forcing that is most consistent with the proxy-based YD signal and the model physics. In our evaluation of the model results, we focus on differences between the last 100-year mean of each experiment and the 13ka reference state (Fig. 1), based on the same variables as provided by the utilized proxy-based reconstructions, i.e. North Atlantic annual SSTs, European July air temperatures, and Greenland annual air temperatures.

We first evaluate the impact of short 1-year long freshwater pulses injected into the Arctic Ocean at the Mackenzie River mouth, in agreement with recent geological evidence[24] and supported by model studies[25-26] (See Supplementary Discussion). To account for uncertainty, we tested fluxes of 0.5 Sv and 5 Sv, and pulse durations of 1 and 3 year (Table 1). Without DA, the 1-year pulses produce no discernible long-term cooling in Europe and the North Atlantic (Fig.1, experiments **1yrS** and **1yrL**), and no long-term AMOC weakening. We repeated these simulations with DA using a particle filter applied annually. This generates much stronger cooling in both these areas of interest, ranging from -0.6 to -0.9°C (Fig. 1, **1yrS_DA** and **1yrL_DA**). Over Europe, the summer cooling is mainly due to an anomalous northerly atmospheric flow, transporting cold polar air southward. This atmospheric shift is associated with reduced surface pressure over Europe and relatively high pressure over the cold North Atlantic, that acts as a blocking for westerly flow (Extended Data Fig. 2b,d). A similar pattern is also generated in a simulation with DA, but without any other change in forcings, but is strengthened by the Atlantic Ocean cooling due to freshwater pulses. Nevertheless, the simulated cooling over Europe is still strongly underestimated compared to the proxies (Fig. 1).

We compare this result with two simulations that evaluate alternative mechanisms without data assimilation: AMOC shutdown and negative radiative forcing. In a first experiment (**SHUTD**), we forced the AMOC to collapse (Extended Data Figs. 3 and 4) by quadrupling the background melt fluxes during 500 years. As expected, this generates intense cooling over both the North Atlantic and Europe, on average by more than 3.5°C (Fig. 1, Extended Data Fig. 3). However, these temperature reductions clearly exceed the reconstructed cooling over both areas. In the second experiment (**RAD10**), we prescribed only a strong negative radiative forcing, obtained by reducing the solar constant by 10 Wm^{-2}. As anticipated, this causes more widespread cooling than the freshwater-induced AMOC perturbations (Extended Data Fig. 3), but in Europe and the North Atlantic the temperature reduction is comparable to **1yrS_DA** and **1yrL_DA** (Fig.1). So, compared to these DA runs with a 1-year freshwater pulse, **SHUTD** and **RAD10** do not produce an improvement of the model-data temperature match. A larger negative radiative forcing would generate stronger cooling that could be closer to the proxy based estimates in Europe and the North Atlantic, but would not match with the relatively mild YD conditions reconstructed in the Southern Hemisphere. Our interpretation is that none of these two mechanisms could be the sole origin of the YD, which is supported by additional experiments performed with different scenarios for freshwater perturbations and radiative forcing and also with different models (see Supplementary Information).

Therefore, as a final step, we applied a combined forcing setup to simulate a climate that is more consistent with proxy-based evidence (Figs. 1 and 2). In this experiment (**COMBINED**), we employed DA and prescribed both a 3-year, 5Sv freshwater pulse and a moderate 2 Wm^{-2} reduction of the solar constant. In addition, this radiative forcing was randomly perturbed after each DA step, for which a 5-year period was selected in this case. The total radiative perturbation in **COMBINED** could represent the impacts of the enhanced atmospheric dust load, and reduced atmospheric greenhouse gas concentrations (see Supplementary Information). In **COMBINED**, we observe considerable changes in the Atlantic Ocean (Fig. 2b), with a southward shift of deep convection, extended Nordic Seas ice cover, and a further AMOC reduction to 7 Sv (Fig. 3c). Over this extended sea-ice cover, air temperatures are 5 to 10°C lower than in the reference state. In the North Atlantic, the associated SST anomalies closely match reconstructions, as both indicate 2.4°C cooling (Fig.1). The simulated atmospheric circulation is similar to the other DA experiments, with anomalous northerly flow over Europe (Fig. 2c). The simulated European cooling of 2.4°C matches reasonably well with the proxy-based average of -1.7°C (Figs. 1 and 2a). We continued **COMBINED** in the same setup for 1000 years, resulting in a state strongly resembling the YD (Fig. 3ab). In **COMBINED**, the particle filter selects and maintains a weakened oceanic state that is most consistent with proxy evidence (Figs. 1 and 3), even when the 3-yr freshwater pulse has finished. Importantly, this state could only be obtained in experiments with DA that combine the three mechanisms (freshwater pulse, radiative forcing and shift in atmospheric circulation), as other combinations either produced a non-stationary state (Extended Data Fig. 5), or a considerable mismatch with the proxy-based reconstructions (see Supplementary Information). After 1000 years we removed the background freshwater forcing, resulting in rapid resumption of the Nordic Seas deep convection, and abrupt warming in the North Atlantic region that closely matches the reconstructed YD termination[16] (Fig. 3).

The **COMBINED** results fit excellently to proxy-based YD evidence in Europe and the North Atlantic region with respect to the magnitude, distribution, duration, and the abruptness of the changes at the start and termination. The simulated temperature anomalies agree also with proxy-based reconstructions from other regions (Extended Data Figs. 6 and 7) and the simulated global cooling of 0.6°C is fully consistent with independent estimates[4]. Based on this excellent model-data match, we conclude that the YD was most likely caused by a combination of 1) sustained severe AMOC weakening due to an initial, short-lived Arctic freshwater pulse and background ice sheet melt, 2) anomalous atmospheric northerly flow over Europe, and 3) moderate radiative cooling related to an enhanced atmospheric dust load and/or reduced atmospheric methane and nitrous oxide levels. The exact magnitude of the forcings at the origin of these three processes or potential interactions between them may depend on our experimental design and requires further investigation. Nevertheless, the need for this particular combination of different processes to explain the observed YD cooling pattern is a robust feature of our analysis (see Supplementary discussion). We regard other mechanisms highly implausible, particularly a full AMOC collapse or a very strong negative radiative perturbation due to an extraterrestrial impact. The origins of abrupt climate change may thus be more complex than previously suggested. Our results may indicate that the YD only occurred due to an unusual combination of events, potentially explaining why the YD was different from preceding stadials. This complexity should be accounted for in studies of past abrupt changes and in analyses of the probability of future climate shifts under influence of anthropogenic forcings.

Methods Summary

We performed our climate simulations with the LOVECLIM1.2 global climate model[27]. This model has been successfully applied in various palaeoclimatic studies, simulating climates that are consistent with proxy-based climate reconstructions, for example for the last glacial maximum, the Holocene, the 8.2 ka event and the last millennium[27], showing that LOVECLIM is a valuable tool in palaeoclimate research. Still, it should be noted that this model has an intermediate complexity. We have performed this study with an intermediate complexity model to be able to make large ensemble experiments with up to 96 members. Compared to comprehensive general circulation models, particularly the atmospheric module has simplified dynamics and low spatial resolution, which limits a detailed representation of the atmospheric circulation. Yet, in the extratropics our model has similar responses to radiative and freshwater forcings as general circulation models (see Supplementary information) . In several of our simulations we applied a particle filter, which is a data-assimilation method to constrain the model results with proxy-based estimates[28-30]. The proxy-based temperatures employed in this study are based on selected quantitative reconstructions from different sources. Details on the model, the experimental design, the particle filter and the proxy-based temperature reconstructions are provided in the Supplementary Information.

References

1. Alley, R. B. *et al.* Abrupt climate change. *Science* **299**, 2005-2010 (2003).
2. Ganopolski, A. & Roche, D.M. On the nature of lead–lag relationships during glacial–interglacial climate transitions. *Quat. Sci. Rev.* **28**, 3361-3378 (2009).
3. Denton, G. H. *et al.* The Last Glacial Termination. *Science* **328**, 1652-1656 (2010).
4. Shakun, J.D. & Carlson, A.E. A global perspective on Last Glacial Maximum to Holocene climate change. *Quat. Sci. Rev.* **29**, 1801-1816 (2010).
5. Clark, P.U. *et al.* Global climate evolution during the last deglaciation. *PNAS* **109**, E1134–E1142 (2012).
6. Shakun, J.D. *et al.* Global warming preceded by increasing carbon dioxide concentrations during the last deglaciation. *Nature* **484**, 49-54 (2012).
7. Steffensen, J.P. *et al.* High-resolution Greenland ice core data show abrupt climate change happens in few years. *Science* **321**, 680-684 (2008).
8. Brauer, A., Haug, G.H., Dulski, P., Sigman, D.M. & Negendank, J.F.W. An abrupt wind shift in western Europe at the onset of the Younger Dryas cold period. *Nature Geosci* **1**, 520-523 (2008).
9. Bakke, J. *et al.* Rapid oceanic and atmospheric changes during the Younger Dryas cold period. *Nature Geosci* **2**, 202-205 (2009).
10. Broecker, W.S., Peteet, D.M. & Rind, D. Does the ocean-atmosphere system have more than one stable mode of operation? *Nature* **315,** 21-26 (1985).
11. Stocker T.F. & Wright, D.G. Rapid transitions of the ocean's deep circulation induced by changes in the surface water fluxes. *Nature* **351**, 729-732 (1991).
12. Rahmstorf, S. Bifurcations of the Atlantic thermohaline circulation in response to changes in the hydrological cycle. *Nature* **378**, 145-149 (1995).
13. Meissner, K.J. Younger Dryas: a data to model comparison to constrain the strength of the overturning circulation. *Geophys. Res. Lett.* **34**, L21705, doi:10.1029/2007GL031304 (2007).
14. Firestone, R.B. *et al.* Evidence for an extraterrestrial impact 12,900 years ago that contributed to the megafaunal extinctions and the Younger Dryas cooling. *PNAS* **104**, 16016-16021 (2007).
15. Wunsch, C. Abrupt climate change: an alternative view. *Quat. Res.* **65,** 191-203 (2006).
16. Heiri, O. *et al.* Validation of climate model-inferred regional temperature change for late glacial Europe. *Nature Commun.* **5**, doi: 10.1038/ncomms5914 (2014).
17. Berger, A. & Loutre, M.F. Insolation values for the climate of the last 10 million years. *Quat. Sci. Rev.* **10**, 297-317 (1991).
18. Stenni, B. *et al.* Expression of the bipolar see-saw in Antarctic climate records during the last deglaciation. *Nature Geosci.* **4**, 46-49 (2011).
19. Manabe, S. & Stouffer, R.J. Coupled atmosphere-ocean model response to freshwater input: comparison to the Younger Dryas event. *Paleoceanography* **12**, 321-336 (1997).
20. McManus, J.F., Francois, R., Gherardi, J.M., Keigwin, L.D., & Brown-Leger, S. Collapse and rapid resumption of Atlantic meridional circulation linked to deglacial climate changes. *Nature* **428**, 834-837 (2004).
21. Barker, S., et al. Extreme deepening of the Atlantic overturning circulation during deglaciation. *Nature Geosci.* **3**, 567-571 (2010).
22. Renssen, H., van Geel, B., van der Plicht, J. & Magny, M. Reduced solar activity as a trigger for the start of the Younger Dryas? *Quat. Int.* **68-71**, 373-383 (2000).
23. Hillaire-Marcel, C., de Vernal, A., Bilodeau, G. & Weaver, A. J. Absence of deep-water formation in the Labrador Sea during the last interglacial period. *Nature* **410**, 1073-1077 (2001).
24. Murton, J.B., Bateman, M.D., Dallimore, S.R., Teller, J.T. & Yang, Z. Identification of Younger Dryas outburst flood path from Lake Agassiz to the Arctic Ocean. *Nature* **464**, 740-743 (2010).

25. Tarasov, L. & Peltier, W.R. Arctic freshwater forcing of the Younger Dryas cold reversal. *Nature* **435**, 662-665 (2005).
26. Condron, A. & Winsor, P. Meltwater routing and the Younger Dryas. *PNAS* **109**, 19928-19933 (2012).
27. Goosse, H. *et al.* Description of the Earth system model of intermediate complexity LOVECLIM version 1.2. *Geosci. Model Dev.* **3**, 603-633 (2010).
28. Dubinkina, S., Goosse, H., Damas-Sallaz, Y., Crespin, E. & Crucifix, M. Testing a particle filter to reconstruct climate changes over the past centuries. *Int. J. Bifurcat. Chaos* **21**, 3611–3618, 2011.
29. Mathiot, P. *et al.* Using data assimilation to investigate the causes of Southern Hemisphere high latitude cooling from 10 to 8 ka BP. *Clim. Past* **9**, 887-901 (2013).
30. Mairesse, A., Goosse, H., Mathiot, P., Wanner, H. & Dubinkina, S. Investigating the consistency between proxy-based reconstructions and climate models using data assimilation: a mid-Holocene case study. *Clim. Past* **9**, 2741–2757 (2013).

Supplementary Information: is available for this paper

Acknowledgements: The research leading to these results has received funding from the European Union's Seventh Framework programme (FP7/2007-2013) under grant agreement no. 243908, "Past4Future. Climate change - Learning from the past climate". HR was supported by a visiting professor grant of the Université catholique de Louvain. HG is Senior Research Associate with the Fonds de la Recherche Scientifique (FRS—FNRS-Belgium). DMR is supported by the Netherlands Organization for Scientific Research (NWO).

Author Contributions: All authors contributed substantially to this work. HR and HG conceived the project. HR, AM, HG and PM designed and performed the LOVECLIM experiments. HR, AM and HG analysed the model results. OH provided proxy-based reconstructions. DMR provided unpublished initial conditions and forcings for the experiments. PJV and KHN performed additional experiments with the HadCM3 and IGSM2 models, respectively. The manuscript was written by HR, with input from all other authors.

Author Information: The authors declare no competing financial interests. Correspondence and requests for materials should be addressed to HR (h.renssen@vu.nl).

Experiments	Duration (yr)	Additional FW forcing (Sv)	Radiative forcing	Ensemble members	Data assimilation
noFW	500	0	0	10	No
1yrS	500	0.5 Sv (1 yr)	0	10	No
1yrL	500	5 Sv (1 yr)	0	10	No
noFW_DA	100	0	0	32	every 1yr
1yrS_DA	100	0.5 Sv (1 yr)	0	32	every 1yr
1yrL_DA	100	5 Sv (1 yr)	0	96	every 1yr
SHUTD	500	4x Backgr FWF	0	10	No
3yrL	100	5 Sv (3 yr)	0	10	No
RAD10	100	0	$-10Wm^{-2}$	10	No
3yrLRAD2	100	5 Sv (3 yr)	$-2Wm^{-2}$	10	No
COMBINED	1500	5 Sv (3 yr)	$-2Wm^{-2}$	96	every 5yr

Table 1. Overview of the experimental design of all perturbation experiments. All experiments were started from a 13 ka **reference state** (See Supplementary Methods) and have been run in ensemble mode, with the number of ensemble members indicated in the fifth column. The freshwater (FW) pulses were added to the Mackenzie River outlet. In all experiments we included a representation of the background melt of the Scandinavian and Laurentide Ice Sheets (Backgr FWF, both amounting 0.05 Sv, see Supplementary Methods). In experiment **SHUTD** this background ice-sheet melt was multiplied by 4. The radiative forcing is included as a reduction of the solar constant by 10 Wm^{-2} (**RAD10**) or 2 Wm^{-2} (**3yrLRAD2** and **COMBINED**), equivalent to a radiative perturbation at the top of the troposphere of respectively -1.75 or -0.35 Wm^{-2}. In **COMBINED**, an additional random radiative perturbation is applied (see Supplementary Methods), resulting because of the DA in a supplementary negative forcing of around -0.17 Wm^{-2}. In **COMBINED** the background melt was removed after 1000 years. Further details on boundary conditions are provided in the Supplementary Information.

Figure legends

Figure 1. Simulated anomalies for European July surface temperatures (in °C, green bars) and annual mean North Atlantic SSTs (in °C, blue bars) from various experiments relative to the 13ka reference experiment, compared with proxy-based reconstructions of 12ka minus 13ka anomalies (far right hatched bars). For details on the experiments, see Table 1 and Supplementary Information.

Figure 2. Simulated anomalies for the **COMBINED** experiment relative to the 13ka reference run: a) upper left, July surface temperatures (in °C), b) upper right, annual mean SSTs (in °C), and c) lower left, July 800 hPa height (in m^2s^{-2}). In our low resolution atmospheric model, the 800 hPa geopotential height (GPH) is considered a better diagnostic for the atmospheric circulation near the surface than sea level pressure (SLP), since GPH is directly calculated by the model whereas SLP is derived from other variables. Positive and negative 800 hPa GPH anomalies directly reflect positive and negative SLP anomalies. These results are 100-year mean values averaged over years 401-500.

Figure 3. Simulated evolution of a) European July Surface temperatures (°C), b) North Atlantic Annual Mean SSTs (°C) , and c) maximum strength of the Atlantic Ocean meridional overturning circulation (in Sv) as a measure for the AMOC strength. The results of the first 100 years are derived from our 13 ka reference simulation. The perturbation experiment **COMBINED** starts in year 101. At year 1101, the background meltwater forcing is removed (see Supplementary Information), leading to a rapid recovery of the AMOC, which is accompanied by warming of the Atlantic Ocean surface and Europe. All results are ensemble means (96 members).

Extended Data Figure legends

Extended Data Figure 1. Proxy-based reconstructions of July surface temperatures (circles), annual surface temperatures (diamonds) annual SSTs (squares) that were used in the data-assimilation. The temperatures are expressed as anomalies at 12 ka relative to the values for 13 ka from the same records. Details on the reconstructions can be found in Supplementary Table 1.

Extended Data Figure 2. Simulated anomalies in July surface temperatures (°C, left column) and July 800 hPa Geopotential heights (m^2s^{-2}, right column), relative to the 13ka reference experiment: **noFW_DA** (a,b), **1yrL_DA** (c,d).

Extended Data Figure 3. Simulated anomalies in July surface temperatures (°C, left column) and July 800 hPa Geopotential heights (m^2s^{-2}, right column), relative to the 13ka reference experiment: **SHUTD** (a,b), and **RAD10** (c,d).

Extended Data Figure 4. Simulated Meridional overturning streamfunction (Sv) for different experiments: a) **spin-up**, b) **13ka reference**, c) **3yrL**, d) **SHUTD**, e) **COMBINED**. Positive values represent clockwise flow. The averages over the last 100 years of each experiment are shown, except for COMBINED, for which the years 401 to 500 are averaged.

Extended Data Figure 5. Simulated evolution of the ensemble mean, maximum AMOC strength (Sv). The results for the first 100 years (black) are identical and represent the **13ka reference** climate. At year 101, this state is perturbed. Shown are the results of **1yrL_DA** (yellow), **3yrL** (blue), **3yrLRAD2** (green), d) **COMBINED** (red). The **COMBINED** experiment has been continued (see main Figure 3). Including the -2 Wm^{-2} perturbation of the solar constant (compare blue and green curves), does not have a discernible impact. Employing data-assimilation (i.e. the difference between green and red curves) results in a continued weakening of the AMOC after the initial perturbation.

Extended Data Figure 6. Simulated global temperature fields (°C). a) July temperature in **13ka reference**, b) annual-mean temperature in **13ka reference**, c) annual-mean temperature anomaly (°C) in **COMBINED** (averaged over years 401-500) relative to the 13ka reference state, with contours at -6, -5, -4, -3, -2, -1, -0.5, -0.25, 0, 0.25, and 0.5°C.

Extended Data Figure 7. Model-data comparison for the annual mean temperature change from the Allerød to the YD plotted against latitude. Four different longitudinal zones are shown: a) 60°W-30°E, b) 30°E-120°E, c) 120°E-150°W, d) 150°W-60°W. The dots represent proxy-based estimates published by Shakun and Carlson (ref. 4, their Figure 12b), with the bars providing a conservative ±1°C uncertainty estimate. The lines are the simulated zonal mean temperature differences between the **COMBINED** experiment (years 401-500) and the 13 ka reference, while the grey shading shows the range of temperatures within the sector.

Extended Data Figure 8. Inter-model comparison of annual mean temperature response to strong negative radiative forcing and AMOC shutdown, relative to a warm control state without any freshwater forcing (see Supplementary Information section 3.4). Figures a, b, e and f reflect the response to strong negative radiative forcing (**RAD10**, solar constant minus 10 Wm^{-2}), while c, d, g and h show the response to an AMOC shutdown (**SHUTD**). LOVECLIM results are shown in the left column (a, c, e, g), HadCM3 results in b and d, and IGSM2 results in f and h. For the comparison with HadCM3, the surface air temperatures are shown, and for IGSM2 the sea surface temperatures, as the latter model includes a zonal statistical-dynamical atmosphere that precludes comparison of atmospheric fields.

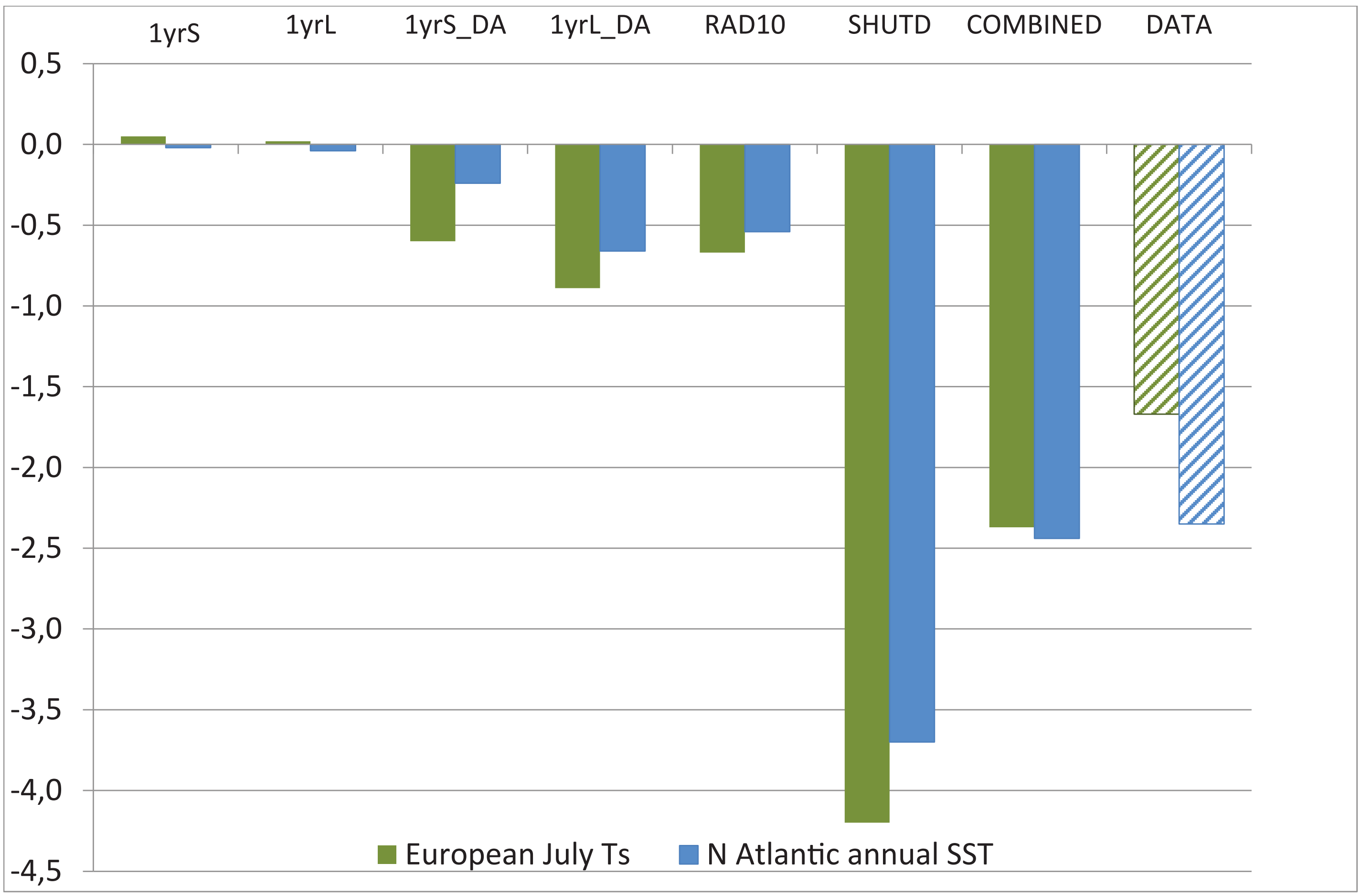

1yrS
1yrL
1yrS_DA
1yrL_DA
RAD10
SHUTD
COMBINED
DATA
0,5
0,0
-0,5
-1,0
-1,5
-2,0
-2,5
-3,0
-3,5
-4,0
-4,5
European July Ts
N Atlantic annual SST

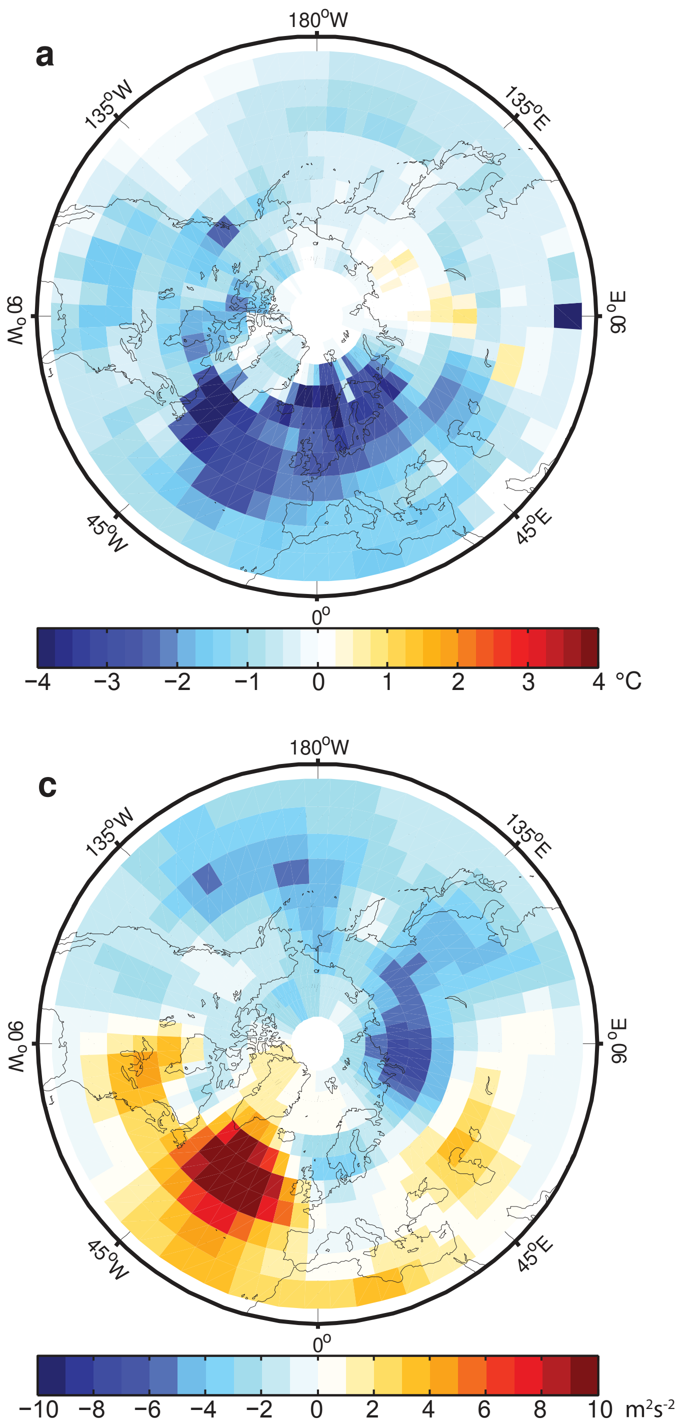

a
180°W
135°W
135°E
90°W
90°E
45°W
45°E
0°
−4
−3
−2
−1
0
1
2
3
4 °C
b
180°W
135°W
135°E
90°W
90°E
45°W
45°E
0°
−4
−3
−2
−1
0
1
2
3
4 °C
c
180°W
135°W
135°E
90°W
90°E
45°W
45°E
0°
−10
−8
−6
−4
−2
0
2
4
6
8
10 m²s⁻²

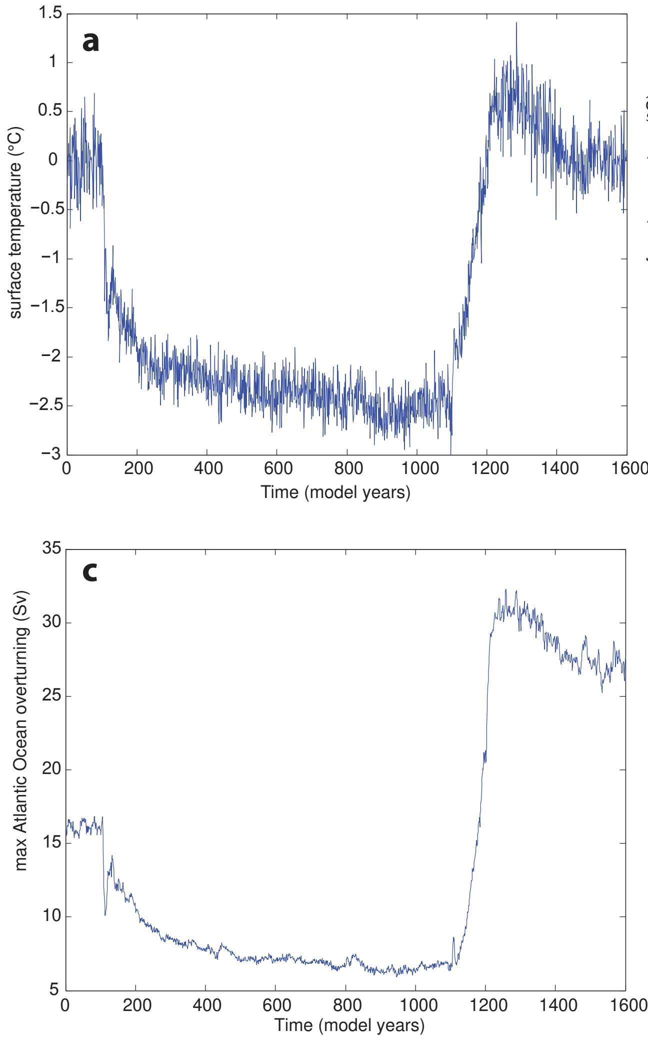

a
b
c
surface temperature (°C)
sea surface temperature (°C)
max Atlantic Ocean overturning (Sv)
Time (model years)

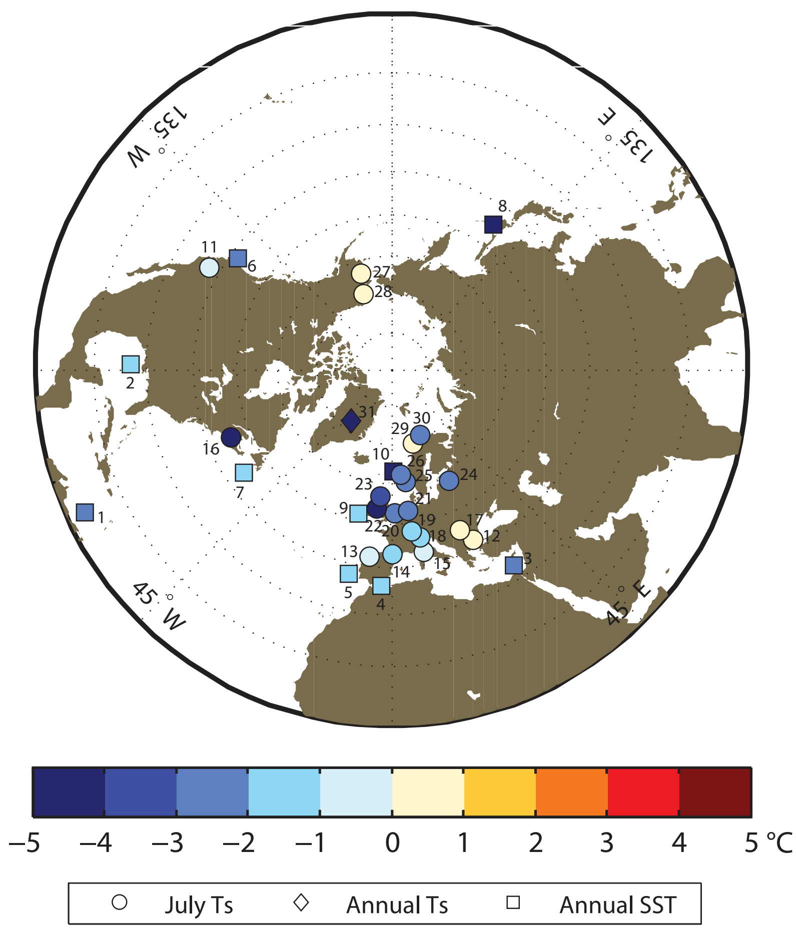
135 °W
135 °E
45 °W
45 °E
1
2
3
4
5
6
7
8
9
10
11
12
13
14
15
16
17
18
19
20
21
22
23
24
25
26
27
28
29
30
31
−5
−4
−3
−2
−1
0
1
2
3
4
5 °C
July Ts
Annual Ts
Annual SST

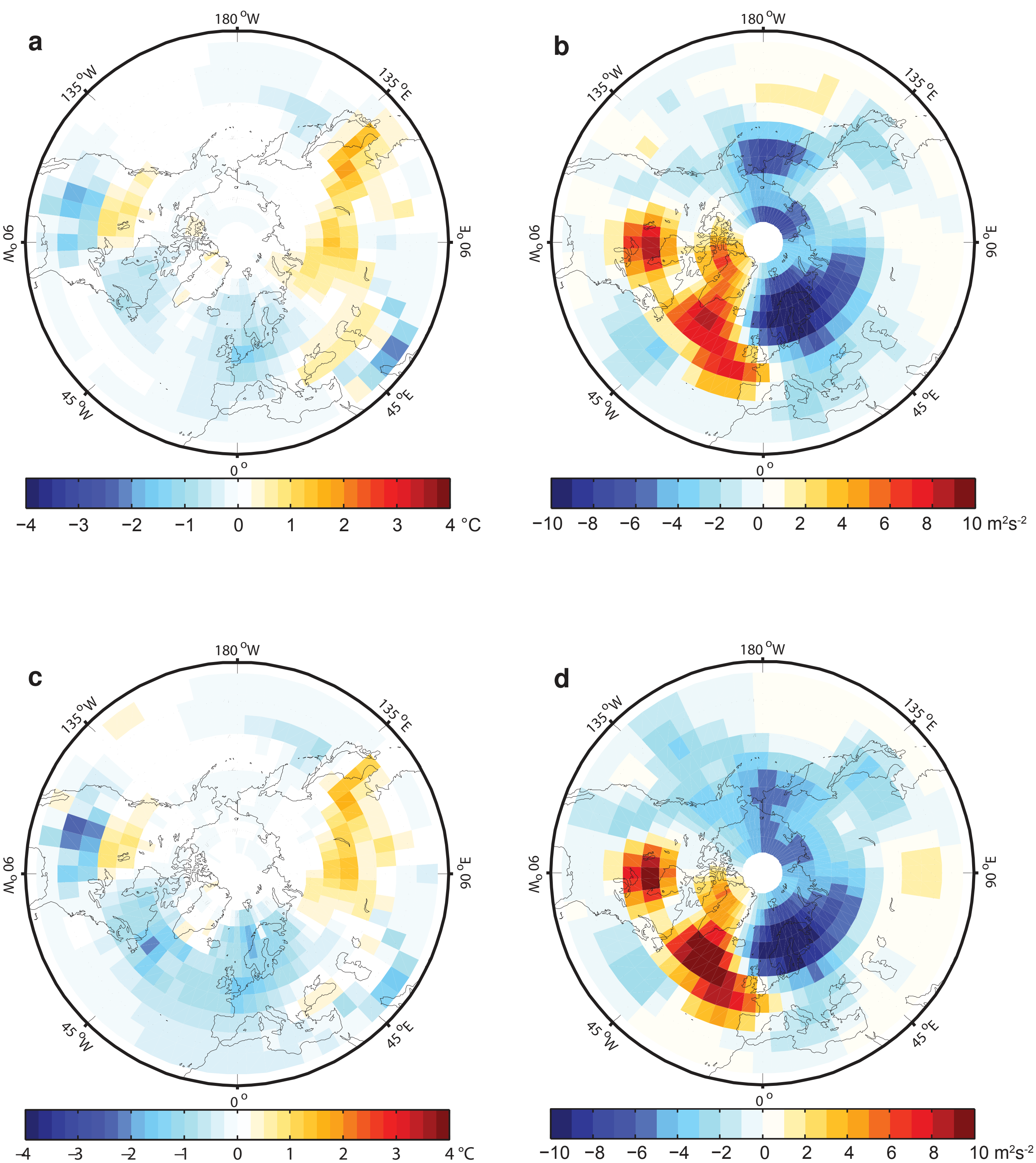
a
180 °W
135 °W
135 °E
90 °W
90 °E
45 °W
45 °E
0 °
−4 −3 −2 −1 0 1 2 3 4 °C
b
180 °W
135 °W
135 °E
90 °W
90 °E
45 °W
45 °E
0 °
−10 −8 −6 −4 −2 0 2 4 6 8 10 m²s⁻²
c
180 °W
135 °W
135 °E
90 °W
90 °E
45 °W
45 °E
0 °
−4 −3 −2 −1 0 1 2 3 4 °C
d
180 °W
135 °W
135 °E
90 °W
90 °E
45 °W
45 °E
0 °
−10 −8 −6 −4 −2 0 2 4 6 8 10 m²s⁻²

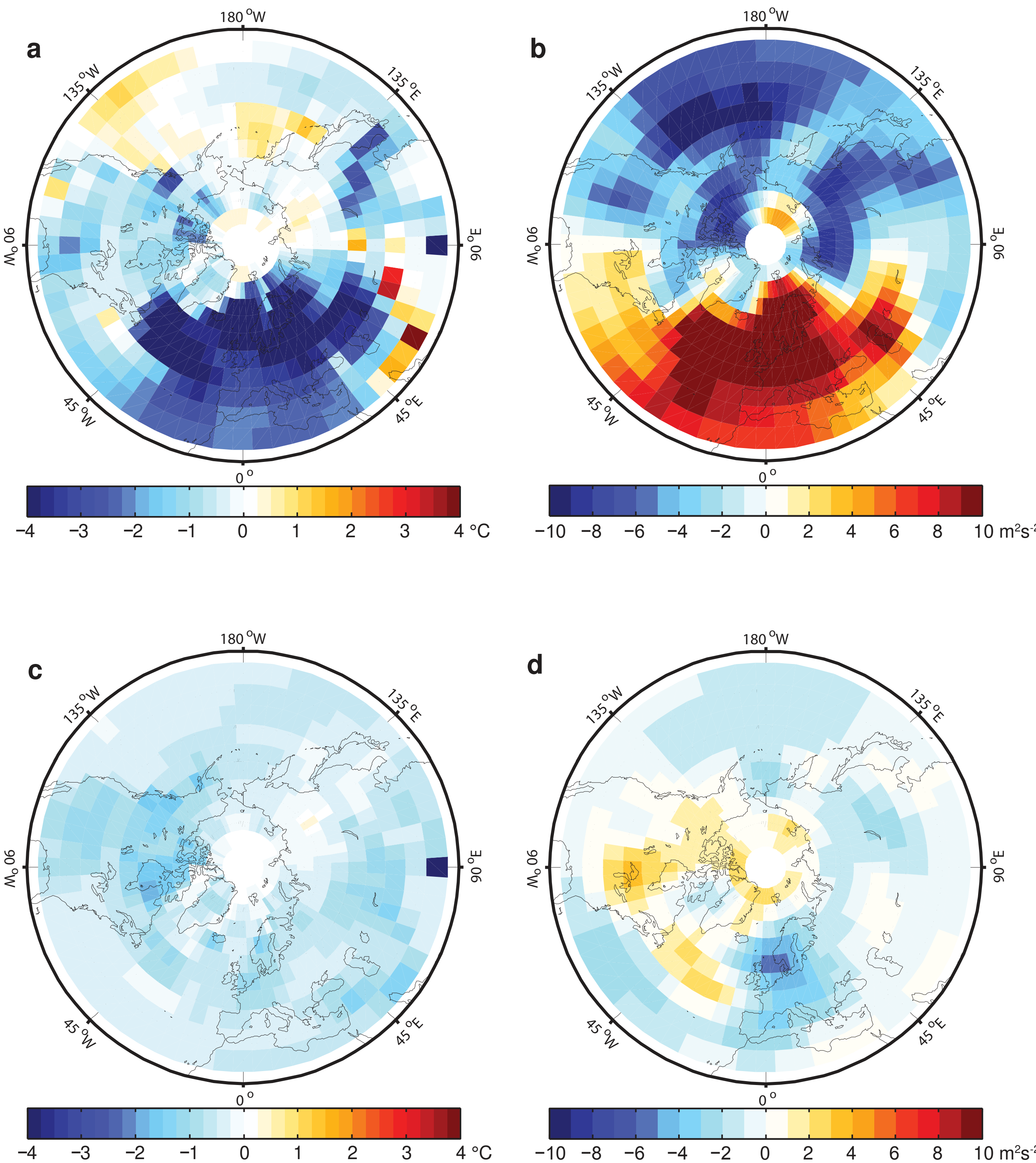

a
b
c
d
180 °W
135 °W
135 °E
90 °W
90 °E
45 °W
45 °E
0 °
−4 −3 −2 −1 0 1 2 3 4 °C
−10 −8 −6 −4 −2 0 2 4 6 8 10 m²s⁻²

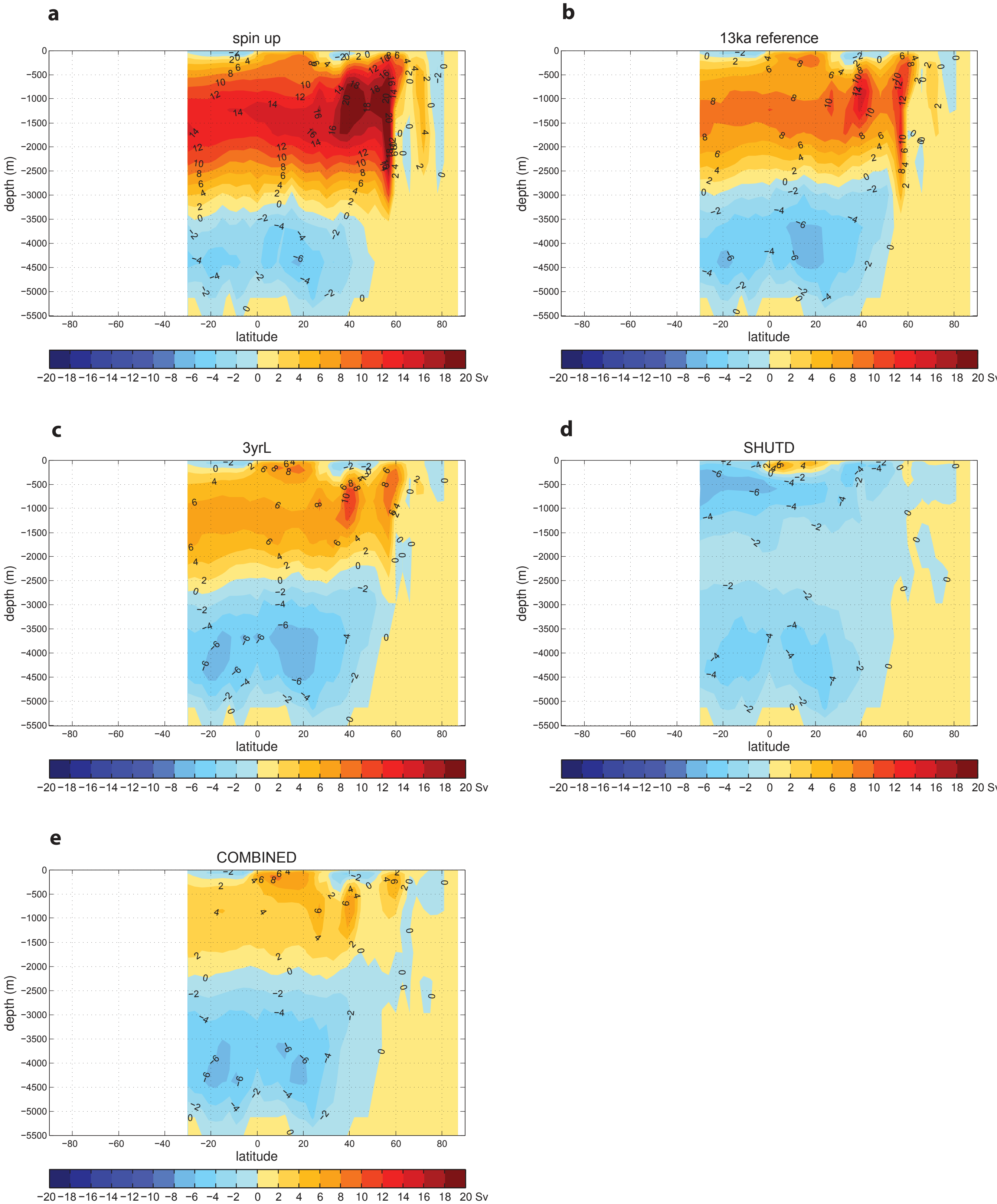
a
spin up
b
13ka reference
c
3yrL
d
SHUTD
e
COMBINED
depth (m)
latitude
0 -500 -1000 -1500 -2000 -2500 -3000 -3500 -4000 -4500 -5000 -5500
-80 -60 -40 -20 0 20 40 60 80
−20 −18 −16 −14 −12 −10 −8 −6 −4 −2 0 2 4 6 8 10 12 14 16 18 20 Sv

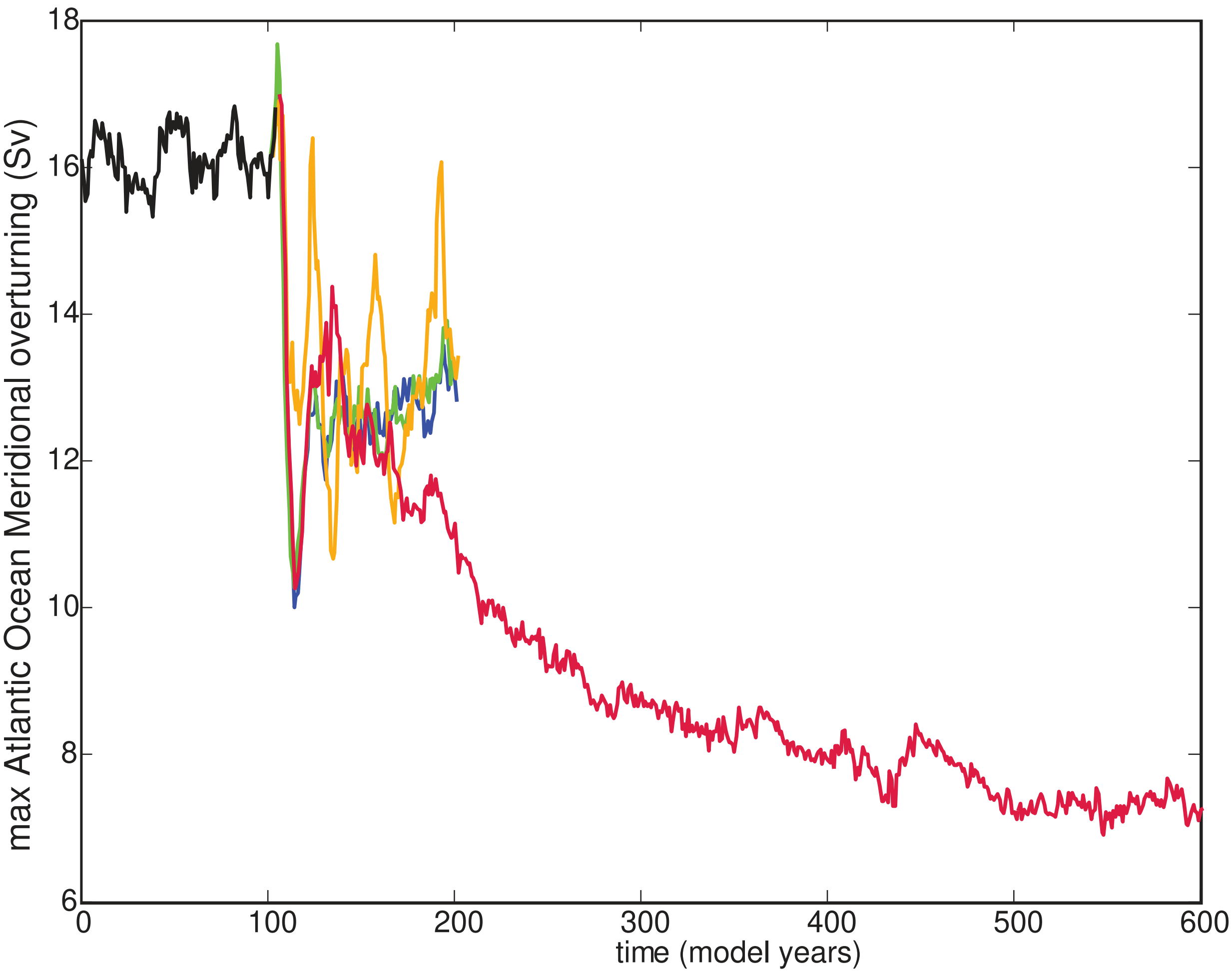

max Atlantic Ocean Meridional overturning (Sv)
time (model years)
18
16
14
12
10
8
6
0
100
200
300
400
500
600

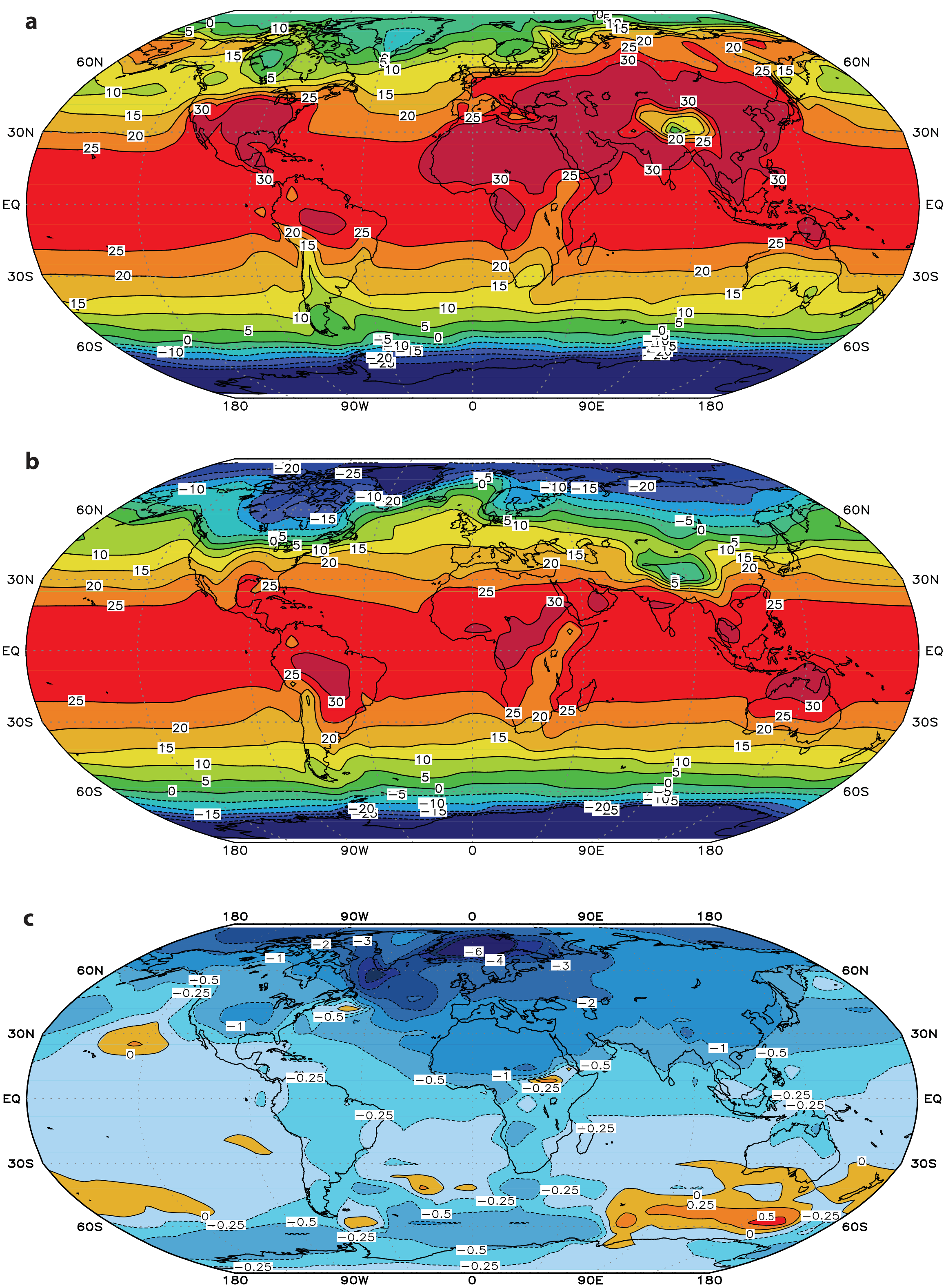
a
60N
30N
EQ
30S
60S
180
90W
0
90E
180
b
60N
30N
EQ
30S
60S
180
90W
0
90E
180
c
180
90W
0
90E
180
60N
30N
EQ
30S
60S

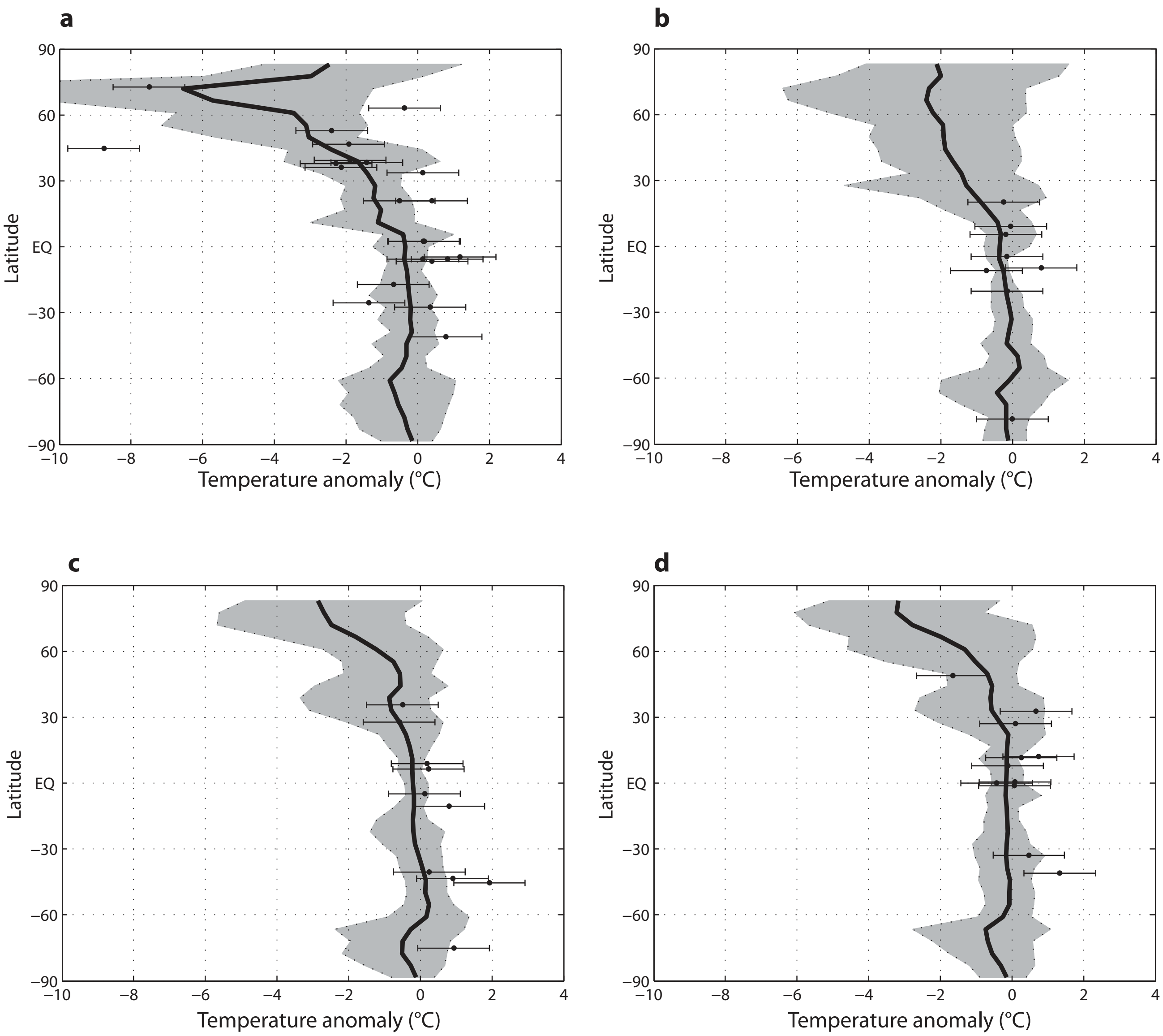
a
b
c
d
Latitude
90
60
30
EQ
−30
−60
−90
−10
−8
−6
−4
−2
0
2
4
Temperature anomaly (°C)

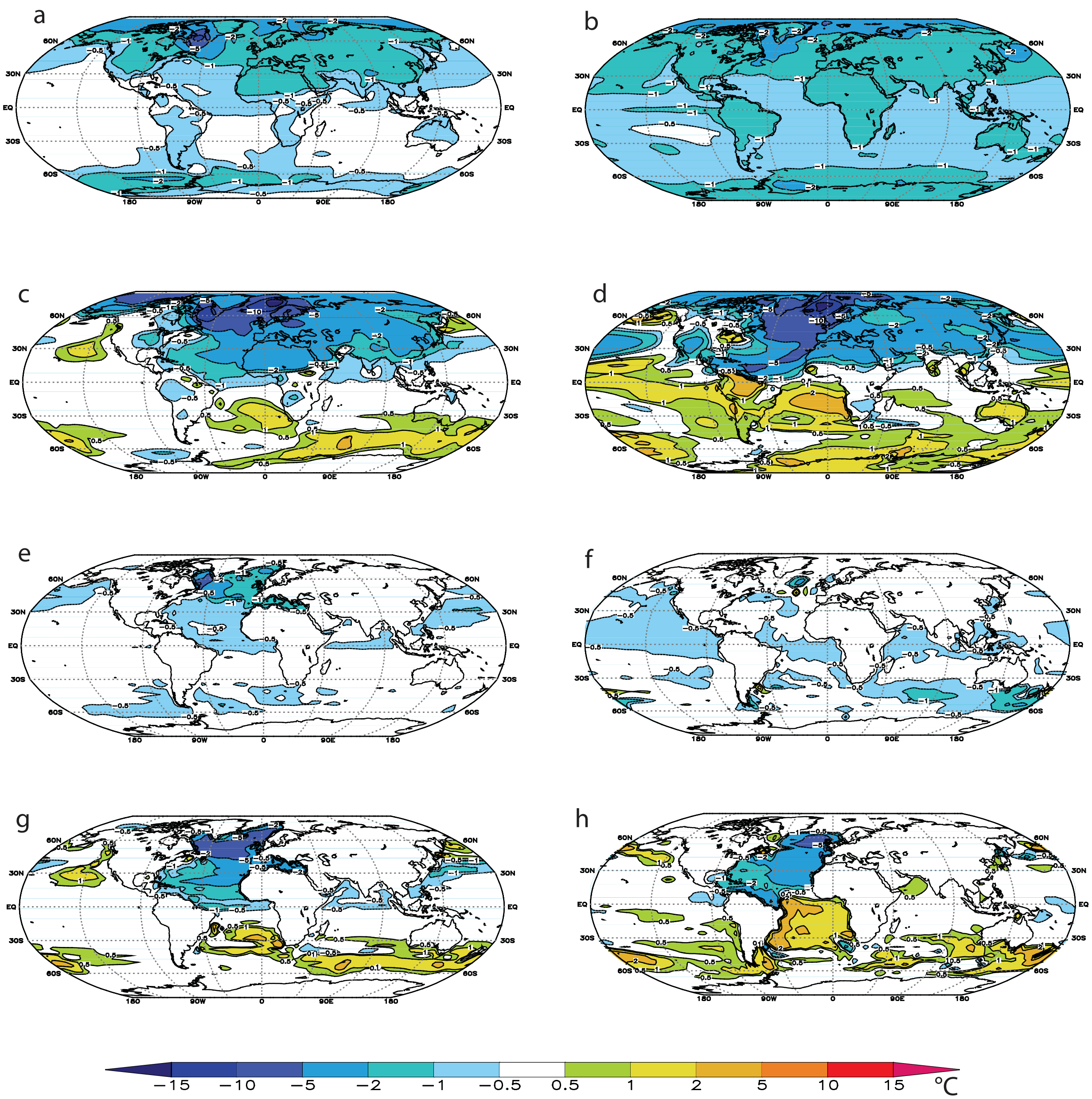
a
b
c
d
e
f
g
h
60N
30N
EQ
30S
60S
180
90W
0
90E
−15
−10
−5
−2
−1
−0.5
0.5
1
2
5
10
15
°C